Detection of Single Nanoparticles and Lentiviruses Using Microcavity Resonance Broadening

Linbo Shao, Xue-Feng Jiang, Xiao-Chong Yu, Bei-Bei Li, William R. Clements, Frank Vollmer, Wei Wang, Yun-Feng Xiao, and Qihuang Gong**

The ability to sense nanoscale objects and biological analytes is particularly crucial for a wide range of applications such as early-stage disease diagnosis, environmental monitoring, emergency response, and homeland security.[1–3] Due to high quality factors (Q) and small mode volumes, respectively describing long intracavity photon lifetimes and strong light confinement, optical resonance devices[4] supporting whispering gallery modes (WGMs) strongly enhance light-matter interactions, and show therefore a lot of promise for ultrasensitive optical biosensing, which monitors the resonance wavelength shift[5–11] or the nanoparticle scattering-induced mode splitting.[12,13] However, the detection signal of the former is very sensitive to various noise such as environmental temperature fluctuations; while the latter has to rely either on ultra-high-Q cavity modes typically approaching or even exceeding 10^8 (refs. 12 and 14), or on high-Q doped microcavities that form narrow-linewidth microlasers.[13] Such ultra-high-Q microcavities have been successfully fabricated in silica, but not in other materials such as polymers and semiconductors widely used in real sensor applications. Here we propose a sensing mechanism by monitoring whispering-gallery mode broadening in microcavities, which is immune to both noise from the probe laser and environmental disturbances, and would remove the strict requirement for ultra-high-Q mode cavities for sensitive nanoparticle detection. Experimentally, the single-nanoparticle-induced mode broadening is demonstrated by one-by-one transferring 70 nm-radius polystyrene (PS) particles to microcavity surface. Furthermore, it holds great potential for measuring single smaller-sized particles, therefore possibly paving the way for practical single molecule microcavity sensing applications.

To precisely measure the mode linewidth, a slightly deformed[15] microcavity is employed such that the cavity mode can be efficiently excited and collected in free space.[16] This removes the extra mode broadening caused by an external near-field coupler such as a tapered optical fiber which is difficult to fully stabilize in experiment. Furthermore, the deformed silica microcavity is coated with a polydimethylsiloxane (PDMS) nanolayer, significantly suppressing the thermo-optic noise induced by both the probe laser and the environmental temperature drift.[17,18] The experimental setup is shown in **Figure 1**a. The probe light is launched from a semiconductor tunable laser (linewidth ≈300 kHz) and then focused on the periphery of the microcavity. The transmitted light is also collected in free space and detected by a low-noise photoreceiver from which the transmission spectrum can be monitored with an oscilloscope (see Experimental Section). The resonance linewidth can be obtained by real-time fitting. In practice, the single-shot measurement time is about 10 ms, limited by the scanning speed of the tunable laser, and can be improved by increasing the scanning speed. The deformed microcavity, serving as the main sensing device in our experiment, inherits the advantages of a circular microcavity including a high Q factor and a small mode volume. As opposed to undeformed cavities, it can be efficiently coupled by a focused free-space beam through chaos-assisted tunneling,[19–21] with the resonant coupling dip depths reaching 75% and 45% for Q ≈10^6 and 10^7 (ref. 15), respectively. Remarkably, the linewidth of the resonant coupling dip does not depend on the coupling strength, as depicted in Figure 1b, which is a dominant advantage compared to external couplers, especially for the linewidth measurement focused on in this work. The microcavity used in the present experiment is fabricated on a silicon wafer by photolithography, silica etching, two-step dry etching, laser reflow, and PDMS coating (see Supporting Information). Figure 1c-e shows scanning electron micrograph (SEM) images of the microcavity with major (minor) diameter of 60 μm (5 μm), where a PS nanoparticle is bound on the cavity surface. In our experiment, to verify the detection ability of the present device and approach, single 70 nm-radius PS nanoparticles are determinately transferred to the microcavity surface one by one from a tapered fiber (see Experimental Section and Supporting Information), and the transfer is finally confirmed by SEM images.

The linewidths of two WGMs with successively bound individual PS nanoparticles are plotted in **Figure 2**a. Their intrinsic linewidths are 54.7 MHz and 143.3 MHz with errors of 582 kHz and 394 kHz, corresponding to intrinsic Q factors of 3.5×10^6 and 1.3×10^6 at the 1550 nm wavelength band, respectively. The transmission spectra of the second mode and the microcavity-enhanced scattering optical images (when excited by a 680 nm laser) with 0 to 4 bound particles are shown in Figure 2b from top to bottom. The transmission spectra are fitted to

L. Shao,[+] X.-F. Jiang,[+] X.-C. Yu, B.-B. Li, W. R. Clements, Prof. Y.-F. Xiao, Prof. Q. Gong
State Key Lab for Mesoscopic Physics and Department of Physics
Peking University, Beijing 100871, P. R. China
URL: www.phy.pku.edu.cn/~yfxiao/index.html
E-mail: yfxiao@pku.edu.cn; qhgong@pku.edu.cn
Dr. F. Vollmer
Laboratory of Nanophotonics & Biosensing
Max Planck Institute for the Science of Light
Günther-Scharowsky-Strasse 1
Erlangen, D-91058, Germany
Dr. W. Wang
Institute of Microelectronics
Beijing, 100871, P. R. China
[+] These authors contributed equally to this work.

DOI: 10.1002/adma201302572

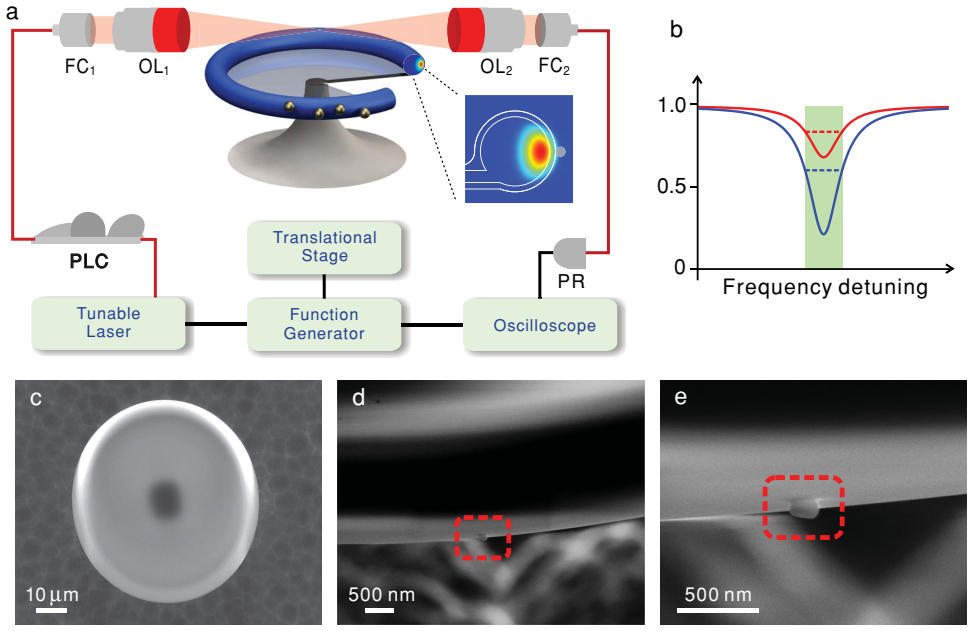

Figure 1. Free-space coupling system for nanoparticles/lentiviruses detection. a) Experimental setup for PS nanoparticles and virus detection using a free-space coupling system. PLC: polarization controller, FC: fiber collimator, OL: objective lens, PR: photoreceiver. Inset: A finite element model of a silica microtoroid with 0.4 µm-thickness PDMS coating. b) Two free-space transmission spectra for different coupling efficiencies, showing the same linewidth. c) SEM image (top view) of a PDMS coated deformed microtoroid. d,e) SEM images of a PS nanoparticle with a radius of 70 nm deposited on the microtoroid surface.

Lorentz lineshapes from which the linewidth of a WGM can be obtained. This fitting procedure is improved by an iteration of weighted least squared regression (see Supporting Information). The maximum mode broadening caused by an individual nanoparticle reaches 23 MHz, while the minimum change exceeds 5.3 MHz which is still one order of magnitude larger than the error of the linewidth measurements. It is noted that the broadenings caused by each nanoparticle are distinct, and depend primarily on the binding positions.[22] In some special cases, the cavity mode may become narrower after a nanoparticle binding event, because the newly-added nanoparticle results in destructive interference that decreases the coupling between the pair of counter-propagating WGMs.[14,22] Real-time detection of nanoparticles using mode broadening in an aqueous environment was also demonstrated (see Supporting Information).

In our experiment, we investigated the uncertainties of single linewidth measurements with different Q factors, as shown in **Figure 3**a. Here the uncertainties (σ) were derived by fitting continuously measured transmission spectra to the standard Lorentz lineshapes, where the expectation value and standard error are obtained. For instance, Figure 3b depicts the fitted linewidths of two modes (A and B) in the absence and in the presence of a single nanoparticle. It can be seen that mode A (B) has an intrinsic mode linewidth of 148.6 MHz (16.8 MHz) and an uncertainty of 2.52 MHz (198 kHz). When a nanoparticle binds to the cavity surface, mode A (B) broadens to 158.0 MHz (25.7 MHz) with an uncertainty of 1.88 MHz (434 kHz). An empirical equation describing the uncertainty of the linewidth measurement can be derived from the experimental data in Figure 3a, $\sigma \simeq (0.0132\Delta\omega + 0.0527)$MHz where $\Delta\omega$ is the cavity mode linewidth, as shown in the black curve in Figure 3a. We conclude that when the Q factors exceed 5×10^6, the uncertainties are predominantly limited by the stability in the scanning process of the probe

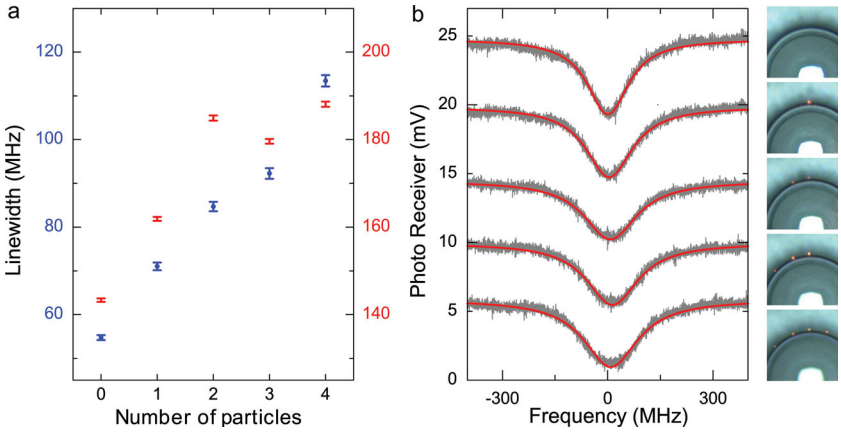

Figure 2. PS nanoparticle-induced mode broadenings. a) Mode broadenings and fitting errors of two resonant modes versus number of bound 70 nm-radius PS nanoparticles. b) Transmission spectra of the mode (intrinsic linewidth ≈143.3 MHz) taken at the 1,550 nm wavelength band. From top to bottom, 0 to 4 bound nanoparticles, and the corresponding microcavity-enhanced-scattering optical images excited by a visible light laser.

Adv. Mater. **2013**,
DOI: 10.1002/adma201302572

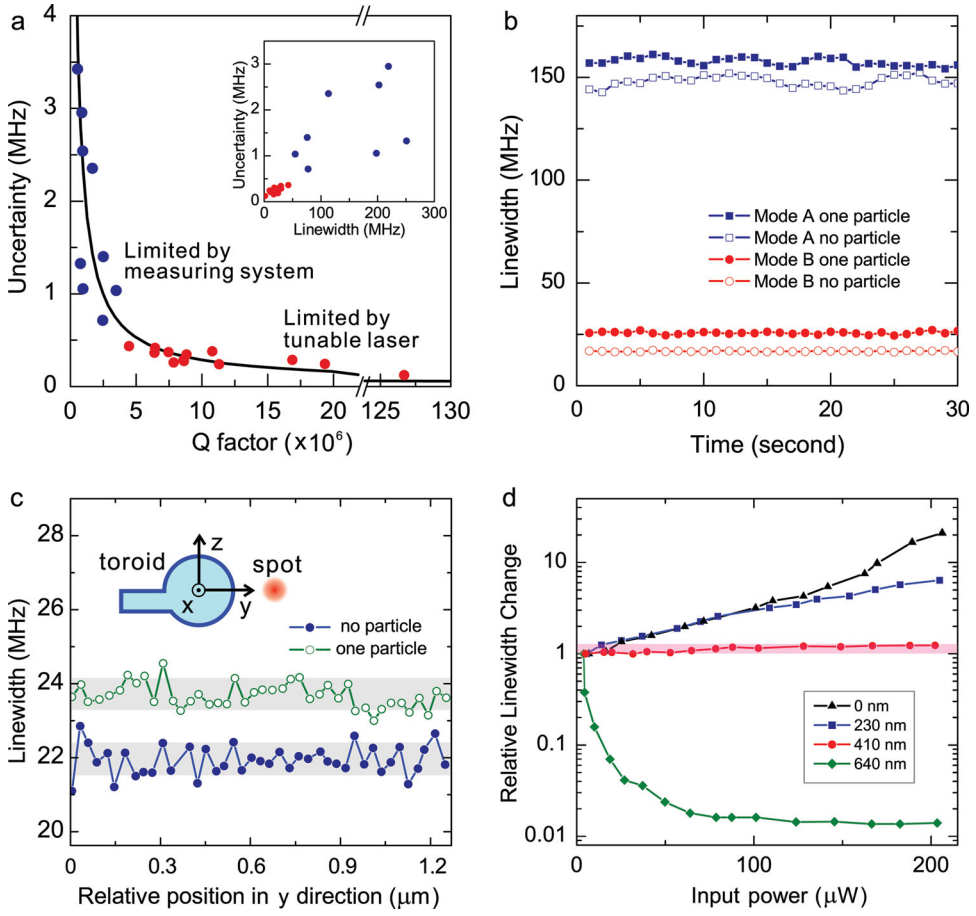

Figure 3. Stability in mode broadening measurements. a) Experimental uncertainties and the corresponding empirical fitted curve of linewidth measurements as a function of the Q factors of cavity modes. Red points: Q factors larger than 4×10^6, the uncertainties of which are limited by the stability of the probe laser. Blue points: Q factors smaller than 4×10^6, the uncertainties of which are determined by the measuring system (≈1.3% of mode linewidths). Inset: the linewidth uncertainties versus the mode linewidths for the same data points. b) Time stability of the linewidths for two modes with and without a single nanoparticle attached on the surface of the microcavity. c) The dependence of linewidths with and without a single nanoparticle on the relative positions Δy of the excitation beam, with coordinates defined in the inset. d) Ratio of measured linewidths of a high Q mode during up-wavelength scans of the probe laser depending on the input power at various coating thicknesses. At the critical thickness of 0.41 μm, the positive thermal refraction effect is compensated completely by the negative thermo-optic PDMS layer.

laser, resulting in a nearly constant uncertainty. It should be noted that the intrinsic linewidth of about 300 kHz of the probe laser only limits the smallest detectable linewidth of the cavity mode, while the uncertainty in the mode linewidth measurement is determined by the stability in the scanning process of the probe laser, which can be less than 300 kHz. The linewidth measurement is a self-referenced measurement, i.e., external drifts do not reduce its accuracy, and thus a best uncertainty of 56 kHz was observed in our experiments. When the Q factors are less than 3×10^6, the uncertainties are on the level of 1.3% of the measured linewidths, which is mainly caused by the electrical measuring system itself including the detection noise from the photoreceiver and the oscilloscope, as well as the distortion of the scanning waveforms applied to the semiconductor laser.

We further investigated the uncertainties depending on the free-space coupling positions and the intensity of the probe laser. First, Figure 3c plots the linewidths measured at different relative positions of the focused beam in the y direction, and that in the z direction is shown in the Supporting Information. These results indicate that the measured linewidths have no obvious change at different coupling strengths. Second, to compensate for the probe-induced positive thermal-optic effect in silica materials,[23] the deformed microcavity is coated with a PDMS nanolayer with a negative thermo-optic coefficient. Other materials, such as poly-p-xylylene, poly-methyl-methacrylate (PMMA), can also be used for biological applications. Figure 3d demonstrates that the thermal-optic mode broadening induced by the probe laser heating has been completely removed at a critical thickness of 410 nm, measured at a cross section cut by focused ion beam (FIB). It should also be noted that the thermal expansion effect is much slower and weaker than the thermo-optic effect, and can be neglected with a fast mode sweeping.

In the last experiment, we demonstrated the ability of sensing lentiviruses in a diluted Dulbecco's modified eagle medium (DMEM). The microcavity was bathed in the sample solution for 120 seconds, then showered with pure and deionized water,

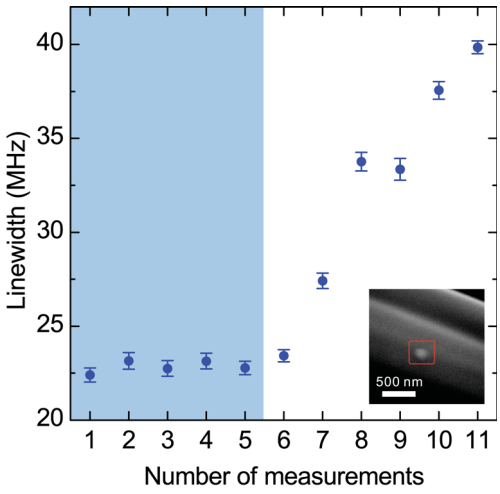

Figure 4. Individual virus detection at ultralow concentrations. A cavity was bathed several times for 120 seconds in two types of DMEM solutions, and the linewidth was measured after each bath. The DMEM solution used for the first five measurements did not contain lentiviruses; the second solution contained lentiviruses with a concentration of 5 fM. Inset: SEM image of a lentivirus deposited on the microtoroid surface.

and finally dried with nitrogen gas (see Experimental Section). The dried microcavity was excited by a free-space laser beam to measure the mode linewidth and assess its uncertainty. In our experiment, the microcavity was first bathed five times in a pure DMEM solution with no lentiviruses, and no obvious mode broadening (<1 MHz) was observed, as shown in the shadowed data of **Figure 4**. The microcavity was then bathed in a solution with a lentivirus concentration of 5 fM. The mode linewidth either did not change (the sixth time and the ninth time) or exhibited evident broadening ranging from 2 MHz to 6 MHz, which is less than the single-virus-induced maximum signal of 7 MHz but significantly exceeds the measurement uncertainty. In addition, considering the ultralow concentration of lentiviruses, there were less than 0.04 lentivirus particles in the cavity volume at any given moment. Thus, we estimated that the measurement in Figure 4 was a single-virus response, and this was finally verified by SEM imaging showing a single lentivirus on the cavity mode area.

The lower detectable limit, i.e., detection limit, depends on the measurement uncertainty σ of the mode linewidth, which can be estimated from the condition

$$\frac{\Gamma}{2\pi} > \sigma \tag{1}$$

The resonance linewidth broadening $(\Gamma/2\pi)$ of the cavity mode caused by a Rayleigh nanoparticle is described by $\Gamma/2\pi = (1/2\pi)(\alpha\omega_c/V_c)(1+\alpha\omega_c^3/(6\pi v^3))f^2(r)$ where α denotes the polarizability of the nanoparticle determined by its physical properties, with ω_c and V_c being resonant frequency and mode volume of the probe mode, $f(r)$ representing the normalized mode distribution at the position r of the particle, and v standing for the speed of light in its surroundings. For convenience of reference, the polarizability of the nanoparticle is given $\alpha = 4\pi R^3(\varepsilon_p - \varepsilon_m)/(\varepsilon_p + 2\varepsilon_m)$ by, where R denotes the radius of the spherical nanoparticle, with ε_p and ε_m being the dielectric permittivities of the nanoparticle and the surrounding medium, respectively. In our experiment, we have $V_c \sim 500\,\mu m^3$, $f(r) \leq 0.26$, $\lambda = 1550$ nm, $\varepsilon_p = 1.592^2$ for PS nanoparticle, $\varepsilon_p \approx 1.45^2$ for lentivirus and $\varepsilon_m = 1^2$ for air. Thus, 20 MHz and 7 MHz linewidth broadenings are expected for the single nanoparticle and lentivirus we used, respectively.

From the experimental results in Figure 3a, the measured uncertainties are approximately $\sigma \simeq (0.0132\Delta\omega + 0.0527)$MHz , and the detection limit can be derived from $\Gamma/2\pi = \sigma$. Thus, the required Q factor can be two orders of magnitude smaller than in mode splitting detection schemes where the splitting signal should be larger than the mode linewidth (see Supporting Information). When the Q factor of the cavity mode is smaller, e.g., 2×10^6 which is suitable for real applications, the detection limit for mode broadening remains about 23 nm, which is still better than that for mode splitting (27 nm) with a Q factor of 10^8. Furthermore, with adequately high Q factors, e.g., exceeding 5×10^7, the smallest detectable nanoparticle is estimated to be smaller than 10 nm. Considering the intrinsic absorption of nanoparticles, the detection limit can be even smaller.

In summary, by employing the nanoparticle-induced mode broadening in a microcavity, we reported detection of individual PS nanoparticles and lentiviruses. This optical detection does not require an ultra-high-Q factor of cavity mode, and has low noise in linewidth measurement with an uncertainty as low as 56 kHz. We envision that individual PS nanoparticles with radii smaller than 10 nm in air environment (15 nm in aqueous environment) are detectable by optimizing experimental conditions with a 30 μm-diameter (60 μm-diameter) microcavity. This means that the present method has the potential to detect single biological protein molecules. In addition, with a narrow and stable linewidth probe laser and by integrating our technique with other enhanced detection methods such as metal nanoparticle enhancement,[24–27] the detection limit of this method can be further improved significantly.

Experimental Section

Fabrication of deformed microtoroids: The microcavity fabrication steps are illustrated in Figure S1 in Supporting Information and explained in the following. (a) The desired photoresist shapes were patterned on a silicon wafer with a 2 μm thermal oxide silica layer by lithography. (b) The silica disks were created by buffered HF etching. (c) The silicon pillars supporting the silica disks were created by isotropic XeF_2 etching. The shape of the Si pillars inherited the shape of the microdisks. (d) The microdisks were then reflowed by a CO_2 pulsed laser, which melted the boundaries of the silica disks and caused them to collapse into toroids with an ultra-smooth surface. (e) A second XeF_2 etching process was used to reduce the top diameter of the Si pillars to reduce the silica-to-silicon loss. (f) Un-solidified PDMS (Sylgard 184, Dow Corning, two parts mixed at ratio of 10:1) droplets were first transferred to a tapered fiber by a fiber tip, and then transferred to the microtoroids to form a thin film of PDMS on the surface of the microcavities, where the thickness of the PDMS coating is determined by droplet size on fiber tip. Finally, the wafer was baked upon a hot plate at 120 °C for 15 minutes to cure this PDMS film.

Free-space coupling system: The coupling system is illustrated in Figure 1a. A laser beam (TLB-6328, New Focus, with a 300 kHz

Adv. Mater. **2013**,
DOI: 10.1002/adma201302572

linewidth), the frequency of which is tunable and modulated by a function generator, was sent through a polarization controller (PLC), a fiber collimator (FC_1), and then was focused by an objective (M Plan NIR 10×, Mitutoyo) on the periphery of the microcavity with a spot size of about 3 μm. The free-space transmission spectrum was collected by another identical objective (OL_2) and a collimator (FC_2), and finally detected by a photoreceiver (Model 1811, New Focus, with a bandwidth of 125 MHz) which was monitored by an oscilloscope (DLM 2034, Yokogawa, with a bandwidth of 350 MHz).

PS nanoparticle transfer: The PS nanoparticle sample (Catalog Number 5014, Thermo Scientific, with diameter of 140 nm) was initially diluted with pure water to a concentration of 10 fM. In our experiment, a tapered fiber was used to transfer individual nanoparticles. First, a fiber taper was immersed into the nanoparticle solution. By sending a visible light laser through the taper and observing light scattering, we monitored nanoparticle binding on the surface of the taper. The taper was then taken out of the solution and the nanoparticles were transferred to the toroid surface by monitoring the scatterings. Finally, SEM was used to check that each nanoparticle had been successfully transferred.

Binding of lentiviruses at ultra-low concentration: The aggregated and detached sample of lentiviruses (Shanghai GenePharma Co., Ltd) was in a DMEM, which contains inorganic salts, amino acids, vitamins, glucose etc. To avoid interference from the medium, a control experiment was performed. The control experiment underwent exactly the same process as the experimental group except that the sample contained no viruses. First, the microcavities were immersed in the droplet sample for 120 seconds, the volume of which was about 20 μL. Second, purified and deionized water was used to shower the microcavity. Since the affinity force between the viruses and the toroid surface was strong, and other substances in the medium were dissolvable in water, only the viruses were attached on the toroid surface after cleaning with water. Then, the chip was dried with nitrogen gas and put on a hot plate at 120 °C for 10 minutes to remove the moisture.

Supporting Information

Supporting Information is available from the Wiley Online Library or from the author.

Acknowledgements

L.S. and Y.F.X. thank Prof. Wensheng Wei, Dr. Junjiao Yang, and Wenjie Xiong at Peking University for help in virus experiments. This work was supported by the 973 program (Grant No. 2013CB328704), the NSFC (Grants No. 11222440, No. 11004003, and No. 1121091), and Beijing Natural Science Foundation Program (Grant No. 4132058). F.V. was funded by the Max Planck Society. L.S. was supported by the National Fund for Fostering Talents of Basic Science (Grant No. J1030310 and No. J1103205), and the Undergraduate Innovational Experimentation Program of Beijing. L.S. and X.F.J. fabricated the microcavities and performed the measurements. X.C.Y. and B.B.L. transferred the PS nanoparticles onto the microcavities. Y.F.X., W.R.C., F.V., W.W. and Q.G. analyzed the data. All authors contributed to the discussion and wrote the manuscript. Y.F.X. conceived the idea and designed the experiment. Y.F.X. and Q.G. supervised and coordinated the project.

Received: June 5, 2013
Published online:

[1] X. Fan, I. M. White, S. I. Shopova, H. Zhu, J. D. Suter, Y. Sun, *Anal. Chim. Acta* **2008**, *620*, 8.
[2] J. N. Anker, W. P. Hall, O. Lyandres, N. C. Shah, J. Zhao, R. P. Van Duyne, *Nat. Mater.* **2008**, *7*, 442.
[3] S. Lal, S. Link, N. J. Halas, *Nat. Photon.* **2007**, *1*, 641.
[4] K. J. Vahala, *Nature* **2003**, *424*, 839.
[5] C.-Y. Chao, L. J. Guo, *Appl. Phys. Lett.* **2003**, *83*, 1527.
[6] A. Yalcin, K. C. Popat, J. C. Aldridge, T. A. Desai, J. Hryniewicz, N. Chbouki, B. E. Little, K. Oliver, V. Van, C. Sai, D. Gill, M. Anthes-Washburn, M. S. Unlu, B. B. Goldberg, *IEEE Journal of Selected Topics in Quantum Electronics* **2006**, *12*, 148.
[7] T. Lu, H. Lee, T. Chen, S. Herchak, J. H. Kim, S. E. Fraser, R. C. Flagan, K. Vahala, *Proceedings of the National Academy of Sciences* **2011**, *108*, 5976.
[8] F. Vollmer, S. Arnold, D. Keng, *Proceedings of the National Academy of Sciences* **2008**, *105*, 20701.
[9] S. Arnold, M. Khoshsima, I. Teraoka, S. Holler, F. Vollmer, *Opt. Lett.* **2003**, *28*, 272.
[10] H. Li, L. Shang, X. Tu, L. Liu, L. Xu, *J. Am. Chem. Soc.* **2009**, *131*, 16612.
[11] H. Zhu, I. M. White, J. D. Suter, P. S. Dale, X. Fan, *Opt. Express* **2007**, *15*, 9139.
[12] J. Zhu, S. K. Ozdemir, Y.-F. Xiao, L. Li, L. He, D.-R. Chen, L. Yang, *Nat. Photon.* **2010**, *4*, 46.
[13] L. He, S. K. Ozdemir, J. Zhu, W. Kim, L. Yang, *Nat. Nano.* **2011**, *6*, 428.
[14] A. Mazzei, S. Götzinger, L. de S. Menezes, G. Zumofen, O. Benson, V. Sandoghdar, *Phys. Rev. Lett.* **2007**, *99*, 173603.
[15] X.-F. Jiang, Y.-F. Xiao, C.-L. Zou, L. He, C.-H. Dong, B.-B. Li, Y. Li, F.-W. Sun, L. Yang, Q. Gong, *Adv. Mater.* **2012**, *24*, OP260.
[16] C. Gmachl, F. Capasso, E. E. Narimanov, J. U. Nöckel, A. D. Stone, J. Faist, D. L. Sivco, A. Y. Cho, *Science* **1998**, *280*, 1556.
[17] L. He, Y.-F. Xiao, C. Dong, J. Zhu, V. Gaddam, L. Yang, *Appl. Phys. Lett.* **2008**, *93*, 201102.
[18] M. Han, A. Wang, *Opt. Lett.* **2007**, *32*, 1800.
[19] J. U. Nockel, A. D. Stone, *Nature* **1997**, *385*, 45.
[20] J. Yang, S.-B. Lee, S. Moon, S.-Y. Lee, S. Kim, T. Dao, J.-H. Lee, K. An, *Phys. Rev. Lett.* **2010**, *104*, 243601.
[21] Y.-S. Park, A. K. Cook, H. Wang, *Nano Lett.* **2006**, *6*, 2075.
[22] X. Yi, Y.-F. Xiao, Y.-C. Liu, B.-B. Li, Y.-L. Chen, Y. Li, Q. Gong, *Phys. Rev. A* **2011**, *83*, 023803.
[23] T. Carmon, L. Yang, K. Vahala, *Opt. Express* **2004**, *12*, 4742.
[24] S. I. Shopova, R. Rajmangal, S. Holler, S. Arnold, *Appl. Phys. Lett.* **2011**, *98*, 243104.
[25] M. A. Santiago-Cordoba, S. V. Boriskina, F. Vollmer, M. C. Demirel, *Appl. Phys. Lett.* **2011**, *99*, 073701.
[26] J. D. Swaim, J. Knittel, W. P. Bowen, *Appl. Phys. Lett.* **2011**, *99*, 243109.
[27] Y.-F. Xiao, Y.-C. Liu, B.-B. Li, Y.-L. Chen, Y. Li, Q. Gong, *Phys. Rev. A* **2012**, *85*, 031805.